The Convective Evolution and Rapid Intensification of Hurricane Earl (2010)

STEPHANIE N. STEVENSON, KRISTEN L. CORBOSIERO, AND JOHN MOLINARI

University at Albany, State University of New York, Albany, New York

(Manuscript received 26 February 2014, in final form 5 August 2014)

ABSTRACT

The relationship between an inner-core ($r < 100$ km) lightning outbreak and the subsequent rapid intensification (RI) of Hurricane Earl (2010) is examined using lightning strikes recorded by the World Wide Lightning Location Network (WWLLN) and in situ observations from various aircraft missions. Moderate ($8.4\,m\,s^{-1}$) northeasterly deep-layer (850–200 hPa) vertical wind shear, caused by outflow from Hurricane Danielle, existed over Earl at the beginning of a prolonged period of RI. Over 70% of the lightning strikes within a 500-km radius occurred downshear, with a preference toward downshear right in the outer rainbands, in agreement with previous studies.

The location of inner-core strikes in Earl differed markedly from previous studies. The inner-core lightning activity precessed from left of shear to upshear, an extremely rare event, beginning just prior to the onset of RI. Diagnosis of the vortex tilt midway through the lightning precession showed this convection was occurring downtilt in the upshear-left quadrant; however, limited observations could not confirm if the vortex tilt was precessing with the lightning. Elevated values of low-level relative humidity and CAPE were also found upshear and supported the inner-core convection, which was found to occur within the radius of maximum wind (RMW). Previous studies have shown that convection located inside the RMW promotes intensification. It is hypothesized that intensification may have occurred in part because the vertical wind shear acted to reduce the upshear tilt, and the occurrence of convection inside the RMW helped to enhance the warm core.

1. Introduction

A clear relationship between lightning activity and tropical cyclone (TC) intensity change has not been established. The analysis of lightning in TCs over the open ocean is a relatively new research area. Although there are numerous regional lightning detection systems in many countries, such as the National Lightning Detection Network (NLDN; Cummins and Murphy 2009) in the United States, a reliable, ground-based, continuous global lightning detection system did not exist until the mid-2000s. Prior to this, lightning data over the open ocean was limited to satellite observations that passed over the same area only once or twice per day. The World Wide Lightning Location Network (WWLLN; operated by the University of Washington) is a global, ground-based network presently consisting of more than 70 sensors that was established in the early 2000s (Lay et al. 2004).

Prior to the WWLLN, many studies examined lightning in TCs using the NLDN. The first study to examine the lightning characteristics of TCs recorded relatively few lightning strikes, but found most of these strikes occurred in the outer rainband region (Samsury and Orville 1994). Molinari et al. (1994) noted that Hurricane Andrew (1992) experienced lightning outbreaks in the eyewall region prior to periods of intensification. A study of nine TCs in the Atlantic basin revealed three distinct regions in the radial lightning distribution: 1) a weak maximum in the eyewall region (<100 km), 2) a clear minimum extending about 100 km beyond the eyewall in the inner-rainband region, and 3) a strong maximum in the outer rainbands (210–290 km) (Molinari et al. 1999). Cecil et al. (2002) found a similar pattern with lightning flash densities 4 times greater in the eyewall and outer rainbands than in the inner rainbands using data from the Tropical Rainfall Measuring Mission (TRMM) satellite's Lightning Imaging Sensor (LIS). These two studies support stratiform rain occurring in the inner rainbands rather than convective rain

Corresponding author address: Stephanie N. Stevenson, Department of Atmospheric and Environmental Sciences, University at Albany, State University of New York, 1400 Washington Ave., Albany, NY 12222.
E-mail: sstevenson@albany.edu

DOI: 10.1175/MWR-D-14-00078.1

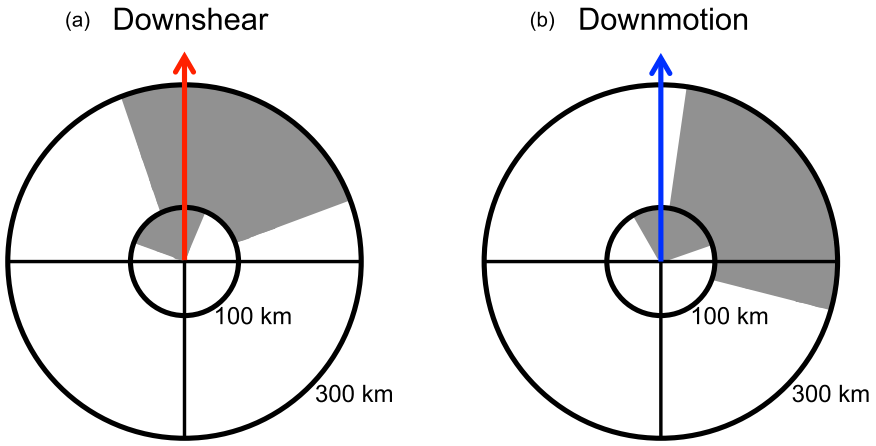

FIG. 1. Regions of maximum lightning frequency adapted from CM03. The shaded gray area indicates where lightning maxima tend to occur in the inner-core (<100 km) and outer rainbands (100–300 km) with respect to (a) shear and (b) motion. The red (blue) arrow represents the direction of shear (storm motion).

(Jorgensen 1984), since lightning is an indicator of deep convection. The three regions of minimum and maximum lightning activity have been replicated in other studies as well (Pan et al. 2010; Abarca et al. 2011).

Corbosiero and Molinari (2002, 2003, hereafter CM02 and CM03, respectively) looked at the azimuthal distribution of lightning in a composite of 35 TCs in the Atlantic basin using the NLDN. These studies related lightning strike locations to both the directions of the deep-layer (850–200 hPa) vertical wind shear and storm motion. When the shear exceeded 5 m s^{-1}, more than 90% of the lightning occurred downshear, consistent with theoretical arguments that shear tilts the TC vortex and induces a stronger diabatic secondary circulation downshear in an attempt to maintain balance and realign the vortex (Reasor et al. 2004). In the inner core (<100 km), lightning frequency peaked in the downshear-left quadrant. In the outer rainbands, there was a strong preference for lightning to peak in the downshear-right quadrant (Fig. 1a). Less than 10% of the inner-core time periods examined, and less than 15% of those in the outer rainbands, had lightning peaks upshear, further emphasizing how strongly the downshear quadrants dominate the lightning distribution. CM03 also found most lightning occurs in the front and right quadrants with respect to motion (Fig. 1b), but ultimately determined this distribution was an artifact of the relationship between the shear and storm motion vectors.

Abarca et al. (2011) performed a similar study to CM02 and CM03 using the WWLLN with 24 TCs in the Atlantic basin. Comparable lightning patterns were found in relation to shear, but motion asymmetries were less clear. This study also concluded that inner-core lightning density has the potential to aid TC intensity forecasts, with forecasts of weaker storms having more potential to benefit from any link between lightning and intensity change, as they tend to have larger lightning flash densities than stronger TCs. Cecil and Zipser (1999) attempted to deduce a lightning and intensity change relationship using the TRMM satellite's optical transient detector (OTD), but with limited passes over each TC, no trends were found.

In recent years, a few studies have begun to look at lightning and intensity trends using the WWLLN. Price et al. (2009) analyzed the strongest TCs (categories 4 and 5 on the Saffir–Simpson scale) in all basins around the globe and found an increase in lightning activity one day prior to peak intensity. Pan et al. (2010) limited their study to seven super typhoons in the northwest Pacific basin and similarly noted lightning outbreaks in the eyewall several hours prior to peak intensity. Pan et al. (2014) expanded the number of northwest Pacific TCs studied to 69, and found peak lightning activity preceded peak maximum sustained winds in 78% of supertyphoons and 56% of weak typhoons. In contrast, a study analyzing Atlantic basin TCs suggested an inner-core lightning outbreak precedes weakening, and an outer rainband lightning outbreak is followed by intensification (DeMaria et al. 2012). Thomas et al. (2010) similarly found increased inner-core lightning activity prior to, and during, periods of weakening in major Atlantic hurricanes. Molinari et al. (1999) proposed two intensity scenarios following an eyewall lightning outbreak. A TC may rapidly intensify if the eyewall lightning outbreak occurs while the TC is weakening, steady, or slowly deepening. In contrast, if the TC has been deepening for some time, an eyewall lightning outbreak may indicate that intensification is coming to an end.

Nearly all studies analyzing lightning in TCs agree that lightning data could help improve intensity forecasts, and it is well known that intensity forecasts have seen little progress over the past few decades (Rappaport et al. 2009). Since there is disagreement over whether a TC will intensify or weaken with an inner-core lightning outbreak, there is a need to analyze this issue further. Lightning activity in TCs is episodic (DeMaria et al. 2012), so analyzing composites of lightning from several TCs may hide important details. Thus, a detailed case study on lightning in an individual TC would add valuable further insight. This study will analyze Hurricane Earl (2010), a case in which an inner-core lightning outbreak preceded a prolonged period of rapid intensification.

A brief background on Hurricane Earl (2010) is given in section 2. Section 3 will discuss the data and methods. Details of the lightning structure in Hurricane Earl (2010) will be discussed in section 4a. Section 4b analyzes the tilt of Earl and the environmental characteristics preceding, and following, the inner-core lightning outbreak. The summary and conclusions will be discussed in section 5.

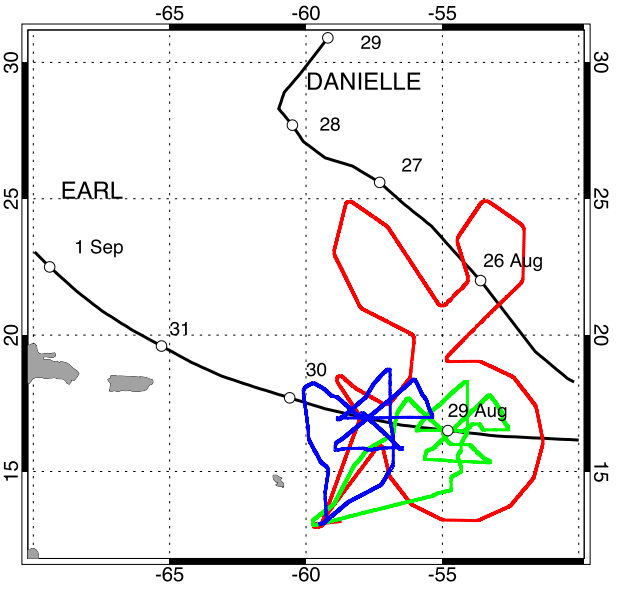

FIG. 2. Interpolated, hourly best tracks for Hurricanes Earl and Danielle (2010). The date is indicated at 0000 UTC each day with a white circle. The colored lines are flight tracks of the data used in this study: NOAA49 (red), NOAA43 (green), and NOAA42 (blue). These flights are near the beginning of RI.

2. Background

Hurricane Earl (2010) formed from a strong African easterly wave that exited the African coast on 23 August. The low pressure became classified as a tropical depression on 25 August and quickly became a tropical storm on the same day. By definition, rapid intensification (RI) is when a TC experiences a 30-kt (1 kt = 0.5144 m s^{-1}) or greater wind increase in 24 h (Kaplan and DeMaria 2003). Earl began to rapidly intensify at 0600 UTC 29 August and continued intensifying until around 0000 UTC 31 August when an eyewall replacement cycle began (Cangialosi 2011). Over this period of RI, Earl went from a 55-kt tropical storm to a 115-kt major hurricane.

Figure 2 shows a portion of the best track data for Hurricanes Danielle and Earl. Although this study does not specifically look at Hurricane Danielle, which also became a major hurricane, the close proximity of the two TCs had an impact on the deep-layer vertical wind shear and environment of Earl at the onset of RI. Also indicated in Fig. 2 are the flight paths of several aircraft that sampled Earl and its environment prior to and during its RI. Several field campaigns [the National Science Foundation's (NSF's) Pre-Depression Investigation of Cloud-Systems in the Tropics (PREDICT), the National Aeronautics and Space Administration's (NASA's) Genesis and Rapid Intensification Processes (GRIP) experiment, and the National Oceanic and Atmospheric Administration's (NOAA's) Intensity Forecasting Experiment (IFEX)] in 2010 helped collect extensive data during the RI of Hurricane Earl; these data are perhaps the most extensive coverage to date for any TC undergoing RI (Montgomery et al. 2014).

3. Data and methods

a. *Lightning analysis*

1) LIGHTNING

The lightning detection system utilized in this study is the WWLLN (http://www.wwlln.com). By late August 2010, at the time of Earl's formation, the WWLLN consisted of approximately 41 "time of arrival" sensors located around the globe [see Fig. 1 in Virts et al. (2013)]. These sensors detect the very low frequency (VLF) radio waves of lightning sferics (Abarca et al. 2011). The VLF energy emitted by a lightning strike travels through the Earth–ionosphere waveguide where it is reflected back and forth to the Earth's surface until it reaches a sensor. This system allows for detection of strikes several thousands of kilometers from the sensor; however, the polarity of the strike is not retained since it is unknown how many times the energy is reflected between the ionosphere and the Earth's surface. The WWLLN is able to capture both cloud-to-ground (CG) and intracloud (IC) strikes, although the detection efficiency (DE) of CG flashes is about twice the DE of IC flashes (Abarca et al. 2010). Lightning strikes identified

TABLE 1. The vertical wind shear direction (meteorological) and magnitude from the GFS and ERA-Interim from 12 h prior to, and after, RI. The shear is calculated from 850 to 200 hPa in a 0–500-km radius from the TC center. The boldface dates indicate the period of RI.

	GFS 1°		ERA-Interim	
	Magnitude ($m\,s^{-1}$)	Direction (°)	Magnitude ($m\,s^{-1}$)	Direction (°)
1800 UTC 28 Aug	7.29	25.59	7.28	19.23
0000 UTC 29 Aug	8.41	45.29	7.57	33.92
0600 UTC 29 Aug	**4.04**	**58.45**	**6.39**	**41.65**
1200 UTC 29 Aug	**7.32**	**40.62**	**8.86**	**43.56**
1800 UTC 29 Aug	**5.38**	**64.07**	**6.55**	**64.07**
0000 UTC 30 Aug	**2.71**	**30.44**	**3.88**	**21.43**
0600 UTC 30 Aug	**2.27**	**325.87**	**4.00**	**52.61**
1200 UTC 30 Aug	**3.18**	**313.40**	**4.62**	**1.79**
1800 UTC 30 Aug	**1.59**	**348.92**	**4.33**	**353.76**
0000 UTC 31 Aug	7.00	328.64	5.03	290.32
0600 UTC 31 Aug	7.42	267.07	8.48	270.26

by the WWLLN have a 10-km location accuracy (Rodger et al. 2009).

In 2003, only 11 WWLLN sensors were active (Lay et al. 2004). This number grew to over 70 sensors in May 2013 (Hutchins et al. 2013). As the number of sensors increases, the DE of the network will increase as well. While the global lightning DE is thought to be around 10% (Abarca et al. 2010), some regions have a higher DE than others. Most notably, Rudlosky and Shea (2013) found that the WWLLN DE is 3 times greater over the ocean than over land when comparing the detected WWLLN strikes to the LIS on board the TRMM satellite. Their study suggests the location where Earl occurred had a DE of approximately 20%. This DE should be interpreted with caution, however, as their study period spanned 2009–12. About 15 sensors were added to the network in the latter two years of their study period, which could lead to the actual DE being lower in late August 2010. Abarca et al. (2011) found that even with a low DE, the WWLLN was able to capture the spatial structure of lightning in TCs quite well when compared to previous studies. For these reasons, the authors believe the WWLLN will provide valuable lightning data in the analysis of the RI of Hurricane Earl.

2) TRACK

The lightning strike locations from the WWLLN were transformed into a storm-centered framework for analysis. The distance of each strike from the center was calculated using the National Hurricane Center (NHC) best track dataset linearly interpolated to 1-min resolution. The track interpolation to each minute was necessary to more accurately map lightning strikes near the core; the strike location relative to the TC center could change quadrants easily if only 6-hourly or interpolated 1-hourly track centers were used. Though the best track is known to miss the erratic behavior of TC movement (Landsea and Franklin 2013), the authors found the lightning distribution patterns, when linearly interpolating the best track to each minute, were very similar to other center location datasets with finer time resolution [e.g., flight reconnaissance data and the Hurricane Research Division's (HRD's) wind center fixes; not shown].

3) SHEAR

Similar to CM02 and CM03, this study will rotate the lightning into a shear-relative framework. Deep-layer vertical wind shear was calculated from 850 to 200 hPa by averaging over a 0–500-km radius from the TC center in order to remove the symmetric vortex (Hanley et al. 2001). Table 1 compares the magnitude and direction of the shear from the Global Forecast System (GFS) 1° analyses and the 0.7° Interim European Centre for Medium-Range Weather Forecasts (ECMWF) Re-Analysis (ERA-Interim). The trends in the magnitude of the shear are similar in both. The direction of shear began similarly in both, from the northeast; however, some discrepancies between the two datasets began to arise toward the end of RI: the GFS switched to northwesterly shear about 12 h prior to the ERA-Interim. The overall distribution of the lightning strikes did not change between the two shear sources despite the directional differences late in the RI period; thus, the authors choose to show results using only the GFS vertical wind shear.

b. Aircraft mission data analysis

In addition to the spatial analysis of the lightning in Earl, aircraft data were used to further analyze reasons for the observed lightning distribution. As previously mentioned, there was extensive flight coverage during the RI of Earl. This study will focus on data from the

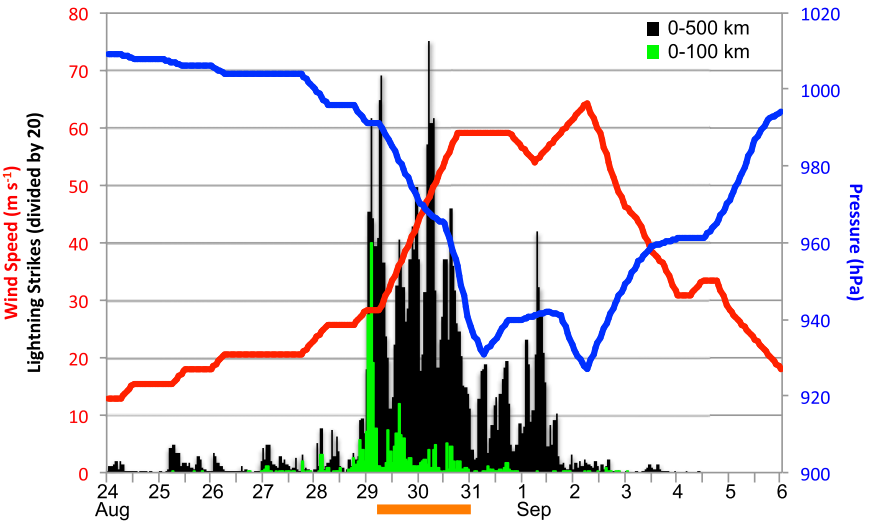

FIG. 3. Wind speed (red; m s^{-1}), pressure (blue; hPa), and lightning strike counts in Hurricane Earl. The dates are labeled at 0000 UTC each day. Both pressure and winds are taken from the NHC best track. The black (green) bars are the number of lightning strikes within 500 (100) km of the TC center. The actual strike count corresponds to the left axis multiplied by 20. The orange line below the time axis indicates when RI (30-kt wind increase in 24 h) occurred, from 0600 UTC 29 Aug to 0000 UTC 31 Aug.

NOAA P-3 aircraft (NOAA42 and NOAA43) and the NOAA G-IV aircraft (NOAA49). The flight tracks of these aircraft are overlaid on the best track in Fig. 2.

1) AIRBORNE DOPPLER RADAR

Airborne Doppler radar wind data were analyzed from two of the NOAA P-3 flights: one prior to RI centered on 0000 UTC 29 August, and another 6 h after RI began centered on 1200 UTC 29 August. The NOAA P-3 gridded Doppler radar winds, with a 5-km grid spacing, were utilized to observe changes in the vortex structure and tilt with height.

Vortex centers were identified by the maximum area-averaged vorticity at each height. Vorticity was calculated from the u and v components of the Doppler winds ($\zeta = dv/dx - du/dy$) and averaged over a 25-km (i.e., five grid points) radius circle to smooth the vorticity field and provide a better estimate of the vortex center. A 25-km radius was chosen because radar data coverage was sparse in several regions of Earl during the first NOAA P-3 flight at 0000 UTC 29 August (see Fig. 8).

2) DROPSONDES

Dropsonde data from the NOAA G-IV and NOAA P-3 flights around 0000 UTC 29 August were analyzed to characterize the environment in which Earl was embedded. While most of the analyzed fields, such as relative humidity or winds, were direct observational measurements, convective available potential energy (CAPE) was also considered. Like Molinari and Vollaro (2010), CAPE values were calculated from a mixed surface layer parcel (0–500 m) with the application of the Bogner et al. (2000) method to correct for saturated, near dry-adiabatic layers below the cloud base.

3) FLIGHT-LEVEL DATA

The flight-level measurements from the NOAA P-3 flights were used to help characterize the inner core of Earl before and during RI. Some of the fields analyzed include the equivalent potential temperature, D values, and wind, which was further decomposed into its radial and tangential components. The D value is the change in height along a constant pressure surface from the standard atmospheric height of that surface, thus a D-value minimum is representative of the TC center.

4. Results

a. *Lightning evolution and structure*

1) OVERVIEW

A remarkable 48 179 lightning strikes were captured by the WWLLN within a 500-km radius over the life span of Hurricane Earl. Only four of the 29 major Atlantic hurricanes from 2005–13 recorded a greater total number of lightning strikes from the WWLLN within the same radius (not shown). Figure 3 shows the evolution of the lightning strikes in Earl from its pretropical

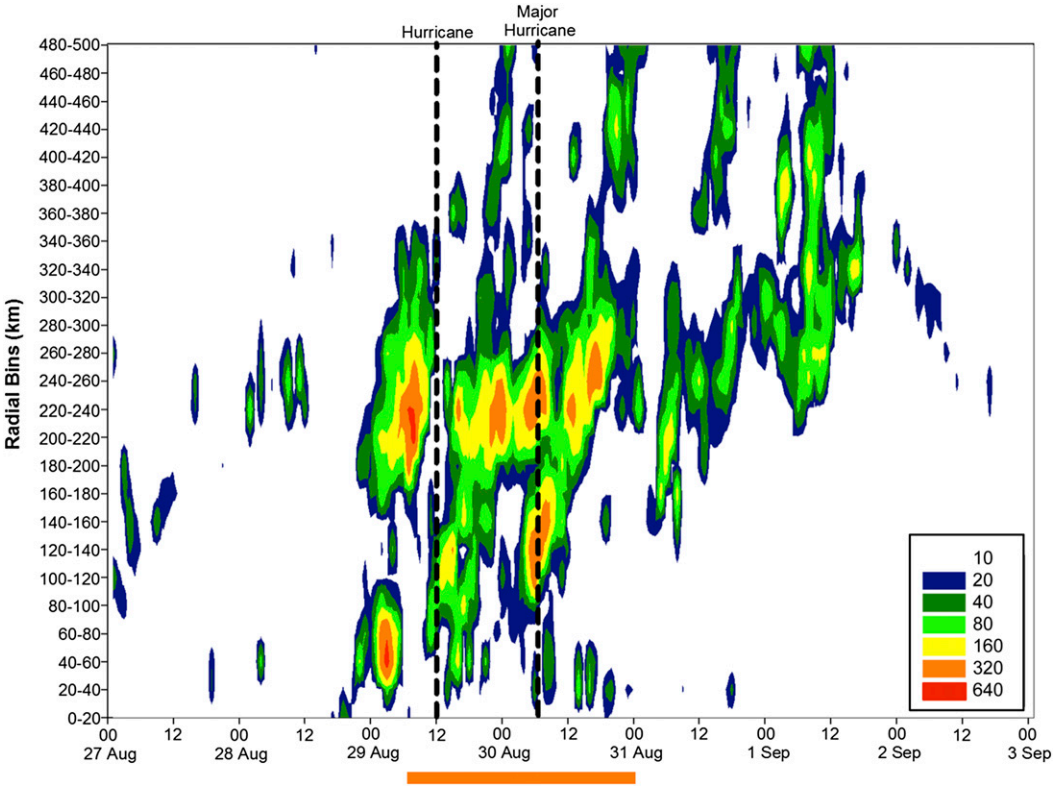

FIG. 4. Hovmöller of the lightning strike frequency every hour in 20-km radial bins extending out to 500 km. The dashed lines indicate when the best track categorizes the cyclone into the specified category on the Saffir–Simpson scale. The orange line below the time axis indicates when RI occurred, from 0600 UTC 29 Aug to 0000 UTC 31 Aug.

depression stage to its extratropical stage. Earl's lightning was not very active until around 0100 UTC 29 August when 800 lightning strikes occurred over the next hour in the inner core. Molinari et al. (2004) noted that the NLDN, which has a much higher DE (70%–90%; Cummins et al. 1998) than the WWLLN, captured almost 900 strikes per hour in the inner core of Hurricane Danny (1997) while the TC was intensifying (see their Fig. 3), the highest strike frequency of any inner-core lightning outbreak within range of the NLDN from 1985 to 2001.

While some studies have suggested inner-core lightning can signal an imminent decrease in TC intensity, Earl seems to suggest inner-core lightning could be associated with intensification, as the burst in Earl preceded a 42-h period of RI (0600 UTC 29 August–0000 UTC 31 August). The pre-RI inner-core lightning burst represented the most significant amount of inner-core lightning during the life span of Earl, as over 60% of the inner-core strikes on 29 August occurred in the 6 h preceding RI. While there were other peaks in the inner-core lightning activity, such as around 1500 UTC 29 August, the amount of strikes in those peaks was less than half of that observed in the pre-RI burst, and was spatially less concentrated in a particular region of the inner core. This point is reiterated in Fig. 4. While Fig. 3 shows the evolution of the number of lightning strikes each hour in two broad radial ranges, Fig. 4 depicts the lightning strike frequency in more detail in relation to the radial distance from the TC center. The inner-core flash count does not exceed 320 strikes per hour at any time during Earl's evolution except during the 6-h period immediately preceding RI. Both figures highlight the extremely active outer rainbands throughout the period of RI. During this period, the outer rainband region experienced over 1000 strikes per hour at its peak. This is consistent with the findings of DeMaria et al. (2012), who found higher lightning flash densities in the outer rainbands correlated to TCs that intensified in the subsequent 24 h.

2) SPATIAL STRUCTURE

Most of the lightning strikes in Earl occurred on the east to southeast side in the inner core, and to the southwest of the TC center in the outer rainbands (Fig. 5a). Earl's motion during RI was toward the west-northwest to northwest. Rotating the lightning strikes to align the motion vector with due north revealed most

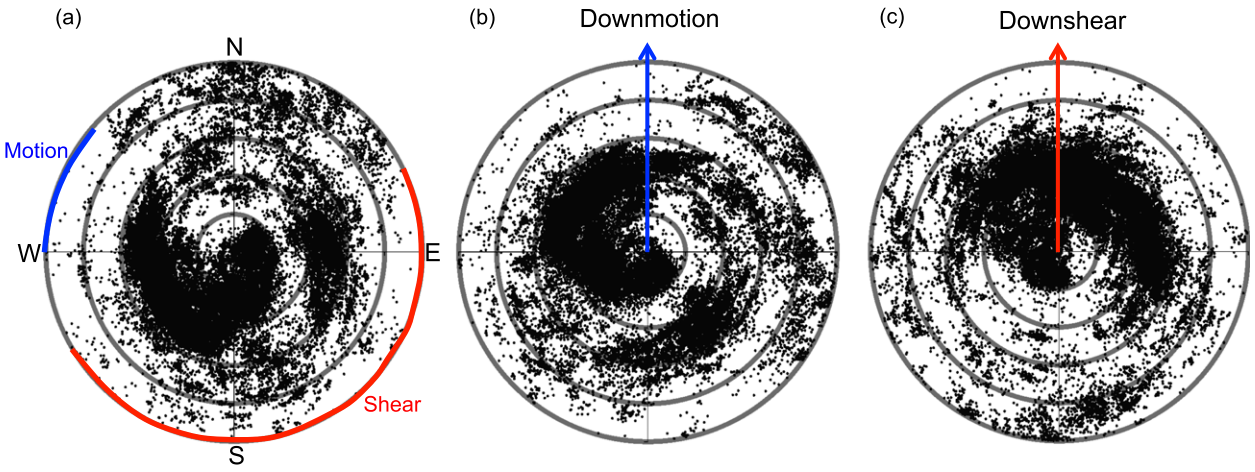

FIG. 5. Lightning strike locations from 2100 UTC 27 Aug to 2100 UTC 31 Aug with respect to (a) Earth, (b) storm motion, and (c) vertical wind shear. Shear is from the GFS analyses and motion is derived from the NHC best track. Range rings (gray) are denoted every 100 km out to 500 km from the TC center. The shaded color regions in (a) represent the varying directions of the northwestward storm motion (blue) and northeasterly, northwesterly, and southwesterly vertical wind shear (red) throughout the time period shown. The lightning strikes were rotated to make the (b) storm motion and (c) vertical wind shear vectors for every 6-h period point due north.

lightning occurred left of motion (Fig. 5b). Many studies have found precipitation (Cline 1926; Miller 1958; Frank 1977; Rodgers et al. 1994) or upward vertical velocity (Jorgensen et al. 1985) maxima right of storm motion. CM03 found most lightning occurs right of motion as well. Their study noted a majority of the cases had a motion vector 0°–90° left of the shear vector. In the case of Earl, the motion vector was 41°–248° *right* of the northeasterly to northwesterly shear vector. Thus, the left of motion lightning maximum, while unusual, is consistent with CM03's determination that shear dominates the azimuthal distribution of lightning in TCs.

The deep-layer vertical wind shear was northeasterly just prior to RI and shifted to northwesterly toward the end of RI (Table 1). Mean vertical wind shear is typically westerly to northwesterly during the summer for this region of the Atlantic basin (Chen et al. 2006). The somewhat unusual shear direction at the beginning of RI was the result of the outflow of Hurricane Danielle located to the north of Earl (Fig. 2). When Earl began RI, Danielle was weakening but still hurricane strength. Rotating the lightning strikes into a shear-relative framework revealed both typical and atypical patterns in the spatial characteristics of the lightning (Fig. 5c). Over 75% of the lightning strikes occurred downshear in the outer rainbands, with a slightly stronger preference for downshear right (44%) versus downshear left (32%), as expected. However, 50% of the inner-core lightning was in the upshear-left quadrant. As previously mentioned, CM03 found it extremely rare for lightning to peak in this particular quadrant (see their Fig. 7); only 4% of the times they analyzed had an upshear-left peak. About 60% of the inner-core, upshear-left lightning strikes in Hurricane Earl occurred in the 6 hours prior to RI.

Focusing on the inner core and the period just prior to RI, Fig. 6b shows the onset and progression of the upshear-left lightning burst in the inner core. The outbreak began around 2100 UTC 28 August left of shear, and increased in intensity as it rotated counterclockwise. The deep convection peaked in lightning production around 0130 UTC 29 August (green dots in Fig. 6b) and continued to rotate around the TC center through the upshear quadrants until about 0600 UTC 29 August. All of this inner-core lightning was located inside the radius of maximum wind (RMW; Fig. 6). The average radial profile of tangential wind for all four of the legs flown through Earl by the NOAA P-3 during the time of the burst is shown in Fig. 6a. While the tangential wind profile was rather flat in Earl, it is clear that the RMW was at least 90 km, if not larger, in the upshear-left quadrant where the lightning burst occurred. This is a rather large RMW, but given that Earl was still a developing tropical storm at the time, it is not unusual.

Shapiro and Willoughby (1982) showed that a heating source (i.e., convection) near the RMW leads to the spinup of the tangential wind just inside the RMW (see their Fig. 11). Musgrave et al. (2012) similarly showed that the tendency of the tangential wind was dependent on the location of diabatic heating relative to the RMW, with diabatic heating located inside the RMW most likely to lead to intensification. Observational airborne Doppler (Rogers et al. 2013) and ground-based (Corbosiero et al. 2005) radar studies have shown that intensifying TCs tend to have convective bursts located inside the

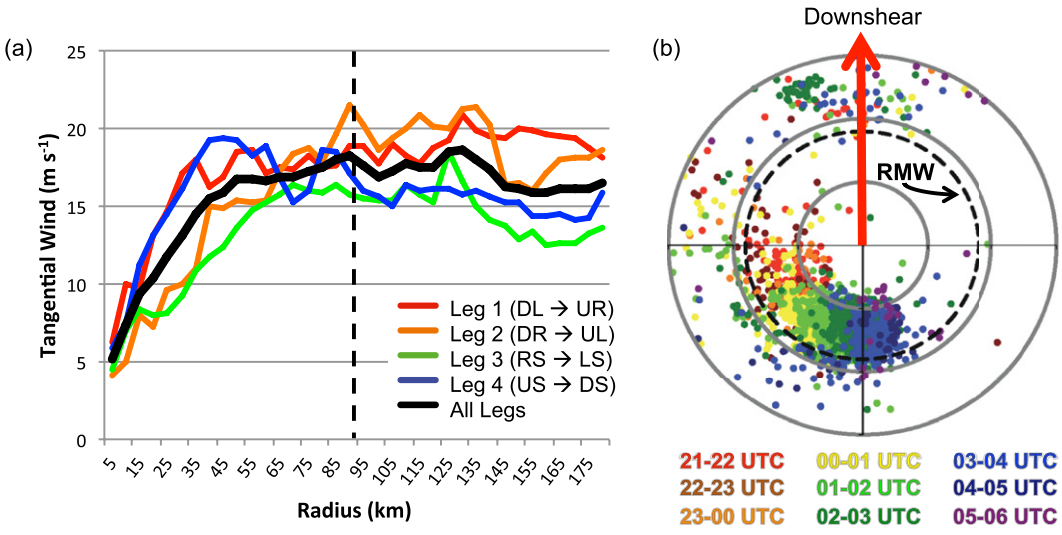

FIG. 6. (a) Average radial profile of tangential wind measured at flight-level (~650–750 hPa) from the NOAA P-3 flight around 0000 UTC 29 Aug. Four individual flight legs averaged from downshear left (DL) to upshear right (UR), downshear right (DR) to upshear left (UL), right of shear (RS) to left of shear (LS), and upshear (US) to downshear (DS) are shown in solid colored lines. The average of these four legs is shown as the solid black line, and the RMW is estimated by the dashed black line. (b) Lightning strike locations in the inner core with respect to the GFS shear vector from 2100 UTC 28 Aug to 0600 UTC 29 Aug. Range rings (gray) are denoted every 50 km out to 150 km from the TC center. The RMW (dashed black line) is from the flight-level data in (a). Colors indicate the hour the strikes occurred.

RMW. Convection, and thus lightning, inside the RMW promotes intensification by further enhancing the warm core through diabatic heating (Vigh and Schubert 2009; Rogers 2010).

The location of the WWLLN lightning strikes matched well with the infrared (IR) coldest cloud tops (Fig. 7). This correlation between lightning and IR imagery demonstrates the ability of the WWLLN to act as a proxy for the location of deep convection in TCs over the open ocean. In Fig. 7a, approximately 3 h prior to the peak of the inner-core lightning burst, an asymmetric cloud shield, defined here as the area with cloud-top temperatures less than −32°C, was evident with a larger shield extending downshear of the TC center and the coldest cloud tops to the left of the shear vector. The inner-core lightning burst began to appear (left of shear) at this time. The next two panels (Figs. 7b and 7c) show the inner-core lightning burst continued to become more intense and slowly rotated counterclockwise around the TC center, leading to an expansion of the cloud shield directly upshear. Additionally, a strong outer rainband developed and took on an arc-like cloud structure downshear of the center with lightning frequency increasing over time (see Fig. 4). By 0600 UTC 29 August (Fig. 7d), when RI was just beginning, the inner-core lightning burst had ceased. Following the inner-core lightning burst, the TC cloud shield became much larger and more symmetric with a very convectively active outer rainband spanning nearly the entire downshear semicircle 200–250 km from the center.

b. *Tropical cyclone and environmental characteristics*

1) VORTEX STRUCTURE

Earl had limited flight coverage prior to RI. During the pre-RI inner-core lightning burst, only one aircraft, the NOAA P-3, was flying through the center of Earl and collecting observations. The flight departed Barbados around 2000 UTC 28 August and flew four legs through Earl's center at ~675 hPa before returning to base around 0400 UTC 29 August. Thus, the data from this aircraft provided the only in situ observations of the vortex structure prior to RI at 0000 UTC 29 August.

Figure 8 shows the airborne Doppler radar-derived area-averaged vorticity at various heights from 0000 UTC 29 August. At 2 and 4 km, the locations of maximum area-averaged vorticity were vertically stacked, approximately 19 km northwest of the HRD surface wind center, which was difficult to define at this time because of Earl's weak intensity (Figs. 8a and 8b). Contrary to the 2- and 4-km maximum area-averaged vorticity centers, the 6- and 8-km maxima were located 38 and 49 km, respectively, to the southeast of the HRD surface wind center (Figs. 8c and 8d). While the lower- and upper-level vortices were weakly connected in the vorticity field (R. F. Rogers, 2014, personal communication), the

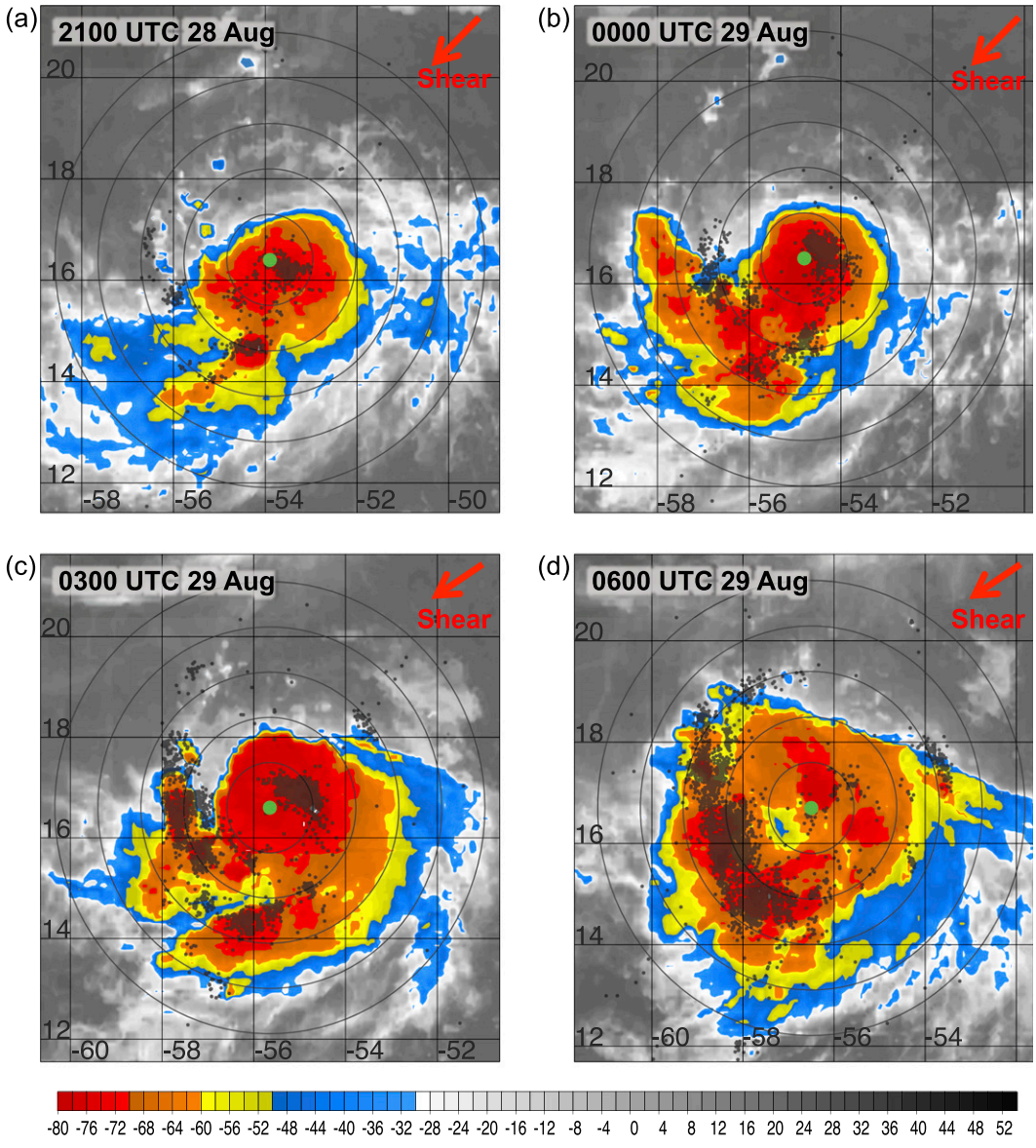

FIG. 7. WWLLN lightning (black dots) and merged IR (GridSat) brightness temperatures (°C). The lightning strikes span 3 h centered on the time of each IR image. The NHC best track center is denoted by the green dot. The GFS shear vector is denoted in the top-right corner of each panel. Range rings are plotted every 100 km extending out to 500 km.

vortex can be characterized as having an upshear-left tilt at this time, as the area-averaged vorticity centers from 2 to 8 km were radially inside the RMW, and the convection responded similarly to the expected theoretical response of a tilted vortex.

Twelve hours later at 1200 UTC 29 August, another NOAA P-3 collected Doppler radar data in Earl. At this time, RI had been under way for 6 h and Earl was now classified as a hurricane. Flight-level measurements showed a contraction of the RMW from 90 km at 0000 UTC to 30 km at 1200 UTC (not shown). The area-averaged vorticity centers were much more aligned at 1200 UTC, with no tilt between the 2-km and 8-km centers, and less than a 10-km tilt between the HRD surface wind center and any height from the surface up to 8 km (Fig. 9).

The upshear tilt that was observed at 0000 UTC 29 August in Earl is atypical for a TC in an environment with moderate vertical wind shear, but it is consistent with the convective activity revealed by lightning locations. Theoretical work has shown vertical wind shear initially acts to tilt the TC vortex downshear, prompting eyewall convection to become asymmetric with a stronger diabatic secondary circulation downshear (Reasor et al. 2004). The downshear tilt of the vortex allows the upper- and

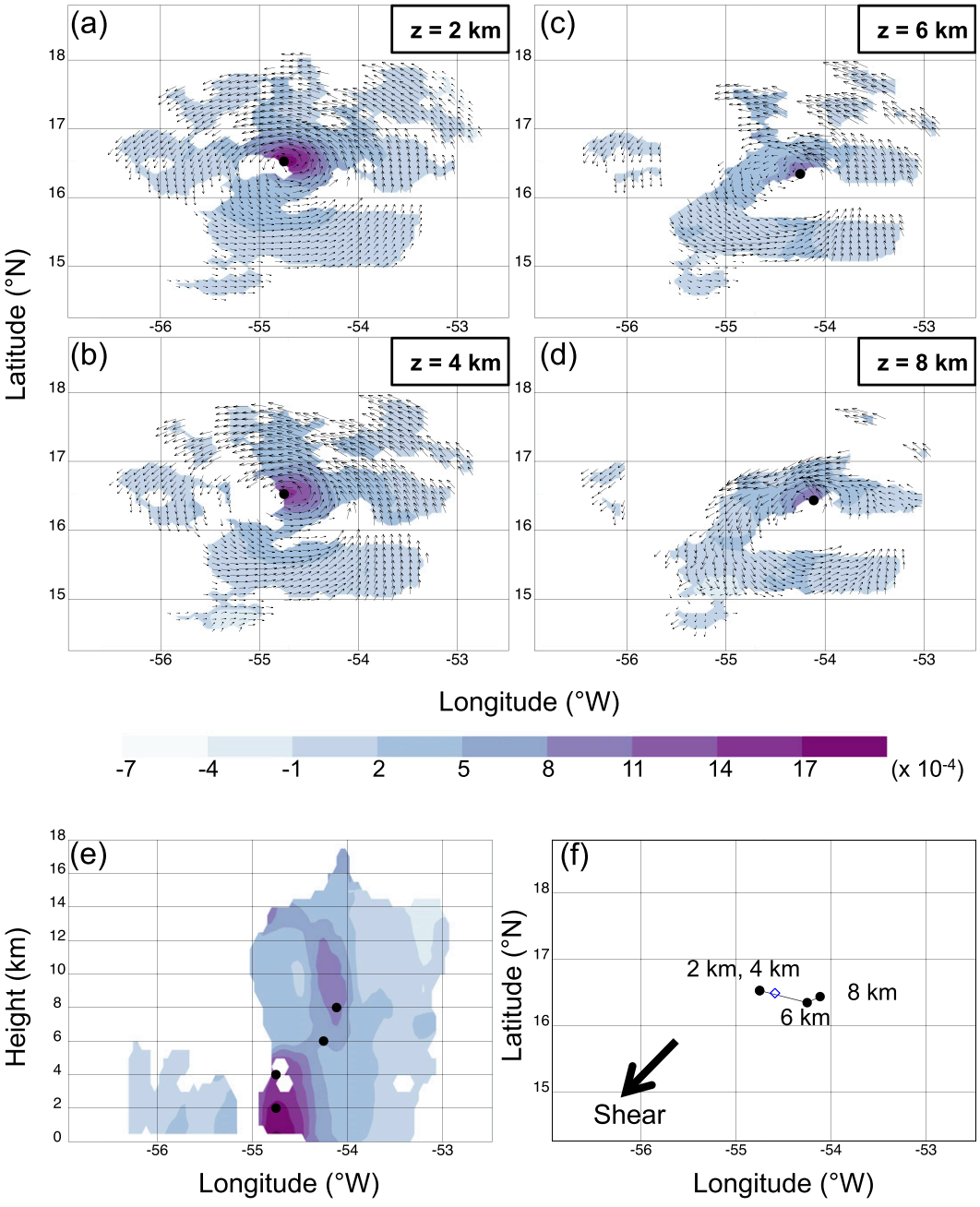

FIG. 8. Area-averaged vorticity (s^{-1}) at 0000 UTC 29 Aug computed from the NOAA P-3 airborne Doppler winds at (a) $z = 2$, (b) $z = 4$, (c) $z = 6$, and (d) $z = 8$ km. The maximum area-averaged vorticity at each height is denoted with a black dot. Wind vectors from the airborne Doppler radar are plotted at each height. (e) A cross section of the area-averaged vorticity through 16.5°N. Maximum area-averaged vorticity centers (black dots) are shown at 2, 4, 6, and 8 km. (f) The maximum area-averaged vorticity points from (a) to (d) to show the vortex tilt. The HRD surface wind center location (blue diamond) is also shown.

lower-level cyclonic potential vorticity anomalies to interact in a manner that results in the cyclonic precession of the tilted vortex. If the vortex precesses upshear, the vertical wind shear would then act to reduce the tilt magnitude (Jones 1995). However, in several numerical modeling studies (Wang and Holland 1996; Rogers et al. 2003; Braun et al. 2006; Wu et al. 2006; Davis et al. 2008), the vortex has been found not to precess all the way around to upshear, but to reach a stable downshear-left configuration, which is optimal for tilt reduction due to

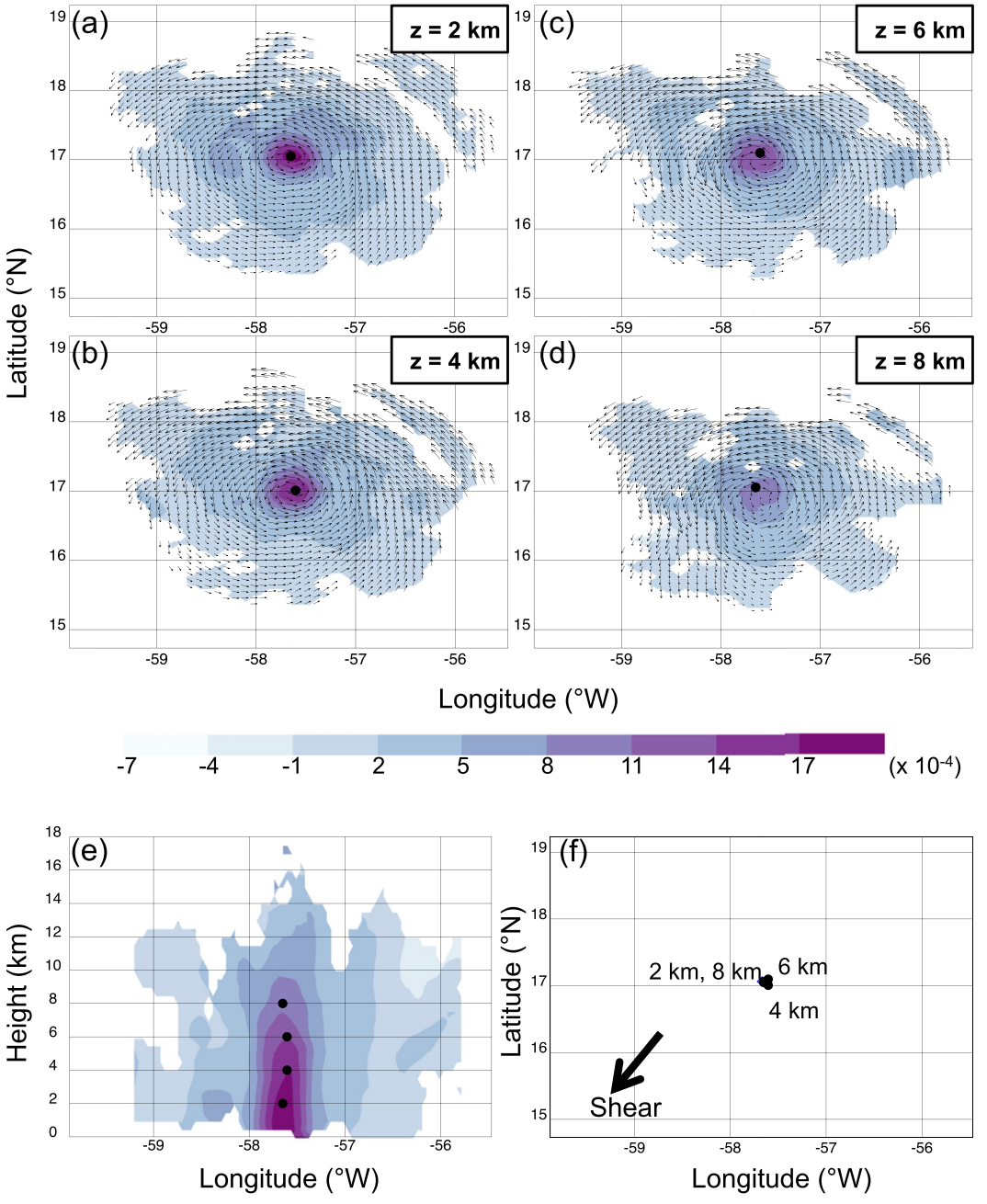

FIG. 9. As in Fig. 8, but for 1200 UTC 29 Aug. The cross section in (e) is through 17.0°N.

the mutual advection of the upper- and lower-level centers (Reasor et al. 2004).

Although continuous observations of vortex tilt are difficult to collect because aircraft need to observe a storm at multiple vertical levels, Reasor et al. (2000) and Reasor and Eastin (2012) were able to use airborne Doppler radar observations from Hurricane Olivia (1994) and Hurricane Guillermo (1997), respectively, and Nguyen and Molinari (2012) used a land-based radar to observe vortex tilt. These three radar-based studies found downshear-left-tilted vortices. Additionally, Reasor et al. (2013) examined airborne Doppler radar data from 19 TCs; almost all of the cases had a vortex tilted downshear, unlike that found here in Earl. While observations were not available to discern if the vortex of Earl was initially tilted downshear, or if the vortex tilt precessed in time, the cyclonically rotating lightning observations at least suggest that the vortex tilt

precessed cyclonically as well. Additionally, the tilt magnitude decreased while the vortex was tilted upshear. Even with the limited data available, the tilt observed suggests the inner-core lightning burst was tied to the direction of tilt rather than the direction of shear, consistent with Jones (1995).

2) TROPICAL CYCLONE AND LIGHTNING ENVIRONMENT

In addition to providing information about the center locations at different levels in Earl, the reconnaissance flights were able to record information about the environment in and around Earl. Around 0000 UTC 29 August, in addition to the NOAA P-3, the NOAA G-IV was flying a reconnaissance mission several hundred kilometers away from Earl's center. Both planes were equipped with dropsondes. Of the 27 dropsondes from the NOAA G-IV flight, 4 sondes were released in each of the downshear-right, downshear-left, and upshear-left quadrants, while only 2 sondes were released in the upshear-right quadrant. These sondes were dropped in the outer rainband region at radii ranging from 250 to 450 km from the TC center. The remaining 13 sondes, approximately 500–1000 km north of Earl's center, captured the environment in the region between Hurricanes Danielle and Earl. Figure 10a shows the average relative humidity (RH) profiles of the 14 ''outer rainband region'' sondes in their respective shear-relative quadrants and the 13 sondes dropped ''north'' of Earl. In the region between the two TCs (north; black line) there is a clear presence of dry midlevel air, with RH values down to 40% near 800 hPa. This dry air appears to have been wrapped into the left-of-shear quadrants by Earl, most clearly upshear left (green line). The RH in this quadrant showed the driest air around 700 hPa at 45%. The low levels, however, were very moist, with RH values approaching 90% below 900 hPa.

These dropsondes, away from the inner core in the outer rainband region, suggest that at radii greater than 250 km, the downshear quadrants were drier at low levels (below 900 hPa) but more moist at upper levels (above 400 hPa) when compared to the upshear quadrants. Molinari et al. (2012) briefly examined the difference in RH upshear and downshear in the 200–400-km radial range using G-IV dropsondes from 32 TCs. They found about 3% *higher* RH downshear below 900 hPa and more than 10% higher RH downshear above 400 hPa. A composite of Atlantic basin TC dropsondes from 1996 to 2012 in the 200–500-km annulus from the TC centers showed a similar pattern at low levels, with RH values 2%–5% higher downshear below 900 hPa (L. T. Nguyen, 2014, personal communication). This suggests that Earl's low levels were unusually dry downshear in comparison to the upshear quadrants. Conversely, the upper levels tended to follow the expected pattern, with larger RH downshear. This result is consistent with the asymmetric cloud pattern in Figs. 7a,b and vertical wind shear advecting high clouds downshear at upper levels.

One could deduce that, given similar temperature profiles among the four shear quadrants (as is the case in Earl; not shown), the more moist low-level air in the upshear quadrants would cause the pseudoadiabatic CAPE to be higher. Figure 11 shows this to be true. Individual sondes are difficult to draw conclusions from, but collectively, the eight downshear sondes had an average CAPE of 1539 J kg^{-1}, while the five upshear sondes (one of the sondes was removed from the CAPE calculations because of multiple levels of missing data) had an average CAPE of 2248 J kg^{-1}. Molinari et al. (2012) found that CAPE in TCs tended to be larger downshear within 400 km of the center, consistent with the convective asymmetries typically observed in TCs. If the high CAPE air observed upshear at outer radii in Earl was transported toward the inner core, it might have created more favorable conditions for deep convection if ascending parcels were able to take advantage of this larger available potential energy.

The NOAA P-3 released 22 dropsondes at radii 0–250 km from the center of Earl around 0000 UTC 29 August. Because of the lower flight level of the P-3, the CAPE values for these sondes could not be calculated to confirm if the high CAPE air located upshear at outer radii was reaching the inner core; however, all four shear quadrants sampled by the P-3 were moist at low levels (Fig. 10b), with upshear left exhibiting 2%–5% higher RH than the other three shear quadrants near the surface. Some of the dry midlevel air appeared to reach the core, though it was not as dry as the outer radii sampled by the G-IV. The lowest RH (60%) seen in the sondes was located downshear left at 700 hPa. Consistent with the G-IV dropsondes, the driest air between 700 and 800 hPa in the P-3 dropsondes was left of shear. Only 7 of the 22 sondes were dropped in the area classified as the inner core ($r < 100$ km), so the RH profiles shown in Fig. 10b are biased toward the environment 100–250 km from the TC center.

One of the NOAA P-3 flight legs was used to examine the environmental characteristics in the vicinity of the inner-core burst. This leg (at approximately 675 hPa) flew from the downshear-right quadrant, through the center, and out through the upshear-left quadrant around 2300 UTC 28 August. Figure 12a shows the D value along the flight path; its minimum around 2250 UTC is representative of the TC center. The tangential wind, also shown in Fig. 12a, confirms the lightning

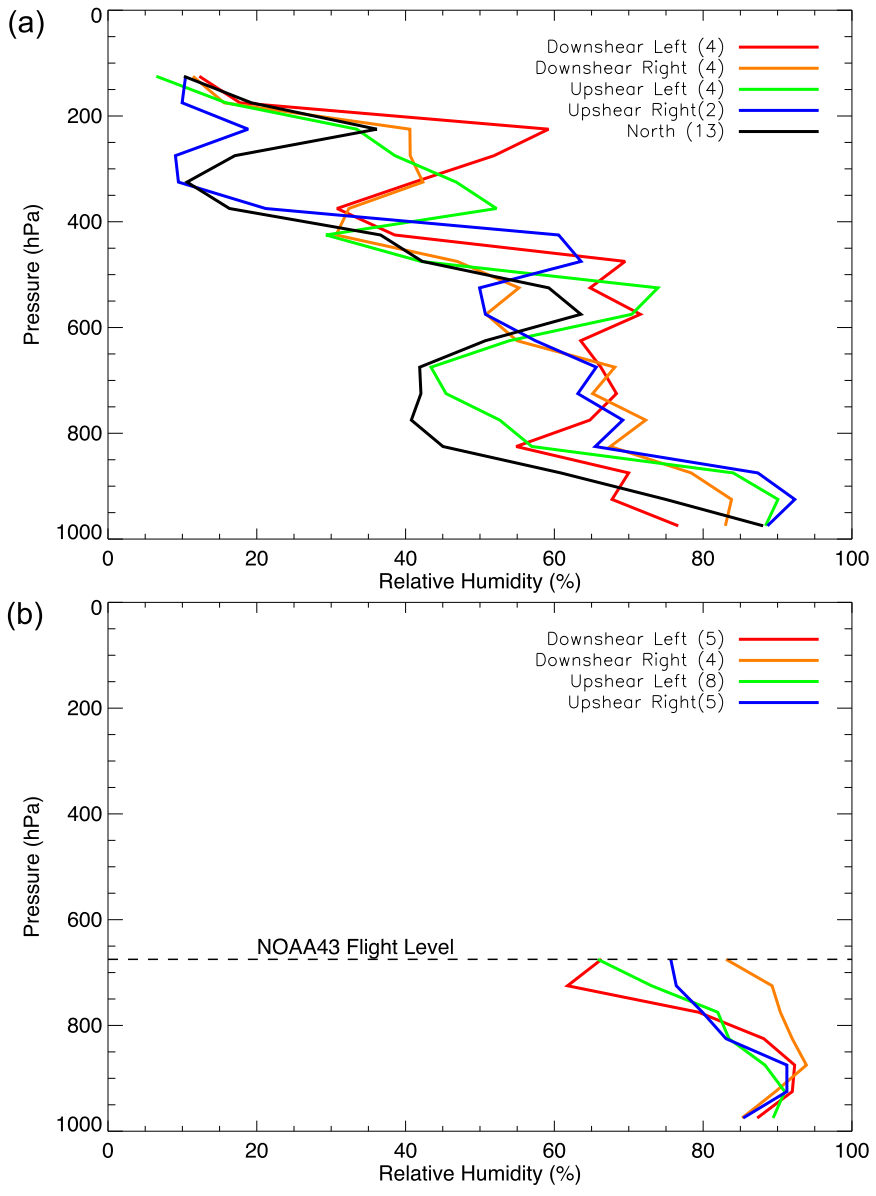

FIG. 10. Average RH (%) from the NOAA G-IV dropsondes (a) 250–450 km from the TC center just prior to RI (2200 UTC 28 Aug–0000 UTC 29 Aug), and from the NOAA43 (b) near the inner core just prior to RI (2200 UTC 28 Aug–0200 UTC 29 Aug) in each of the shear quadrants and in the region between Hurricanes Danielle and Earl to the north of Earl's center. Averages were computed in 50-hPa bins. The number in parentheses in the legend represents the number of dropsondes averaged for each quadrant or region.

burst was located radially inward of the RMW in the upshear-left quadrant. Flight-level data revealed a transition from positive (outflow) to negative (inflow) radial winds in the region where the inner-core lightning burst occurred, upshear left of the TC center (Fig. 12c), implying convergence at flight level. Coincident with this radial wind sign reversal, a sharp gradient in equivalent potential temperature θ_e was found (Fig. 12b). Corbosiero et al. (2005) similarly found that the maximum negative radial gradient in θ_e coincided with the location of the maximum eyewall updraft in Hurricane Elena (1985). A sonde dropped 14 km from the center in the upshear-left quadrant of Earl showed inflow of about 5 m s^{-1} transitioning to outflow above 800 hPa (not shown). Another sonde dropped in the same quadrant, 98 km from the TC center, showed approximately 10 m s^{-1} of inflow at low levels that began transitioning to outflow near flight level at 760 hPa. Inflow at low levels and outflow at midlevels

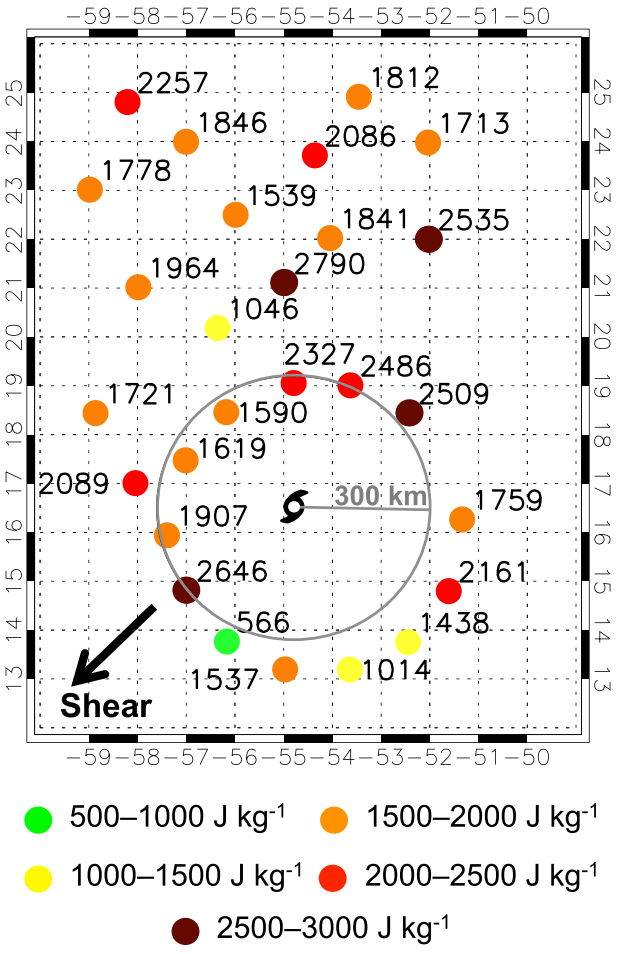

FIG. 11. CAPE values calculated from the NOAA G-IV dropsondes just prior to RI from 2200 UTC 28 Aug to 0000 UTC 29 Aug. Colors indicate the CAPE magnitude. The NHC best track surface center for 0000 UTC 29 Aug is indicated by the tropical storm symbol, with the 300-km range ring (gray) also shown. The GFS shear vector at this time is shown in the bottom-left corner.

suggests upward motion to complete the outward-sloping secondary circulation. The flight level radial winds and sharp θ_e gradient both support the occurrence of deep convection and lightning on the upshear-left side of the TC.

5. Summary and conclusions

Continuous global lightning datasets are in the early stages of being feasible for research purposes. Although continental lightning detection networks have previously been used to investigate the lightning structure in TCs, few have examined lightning in tropical cyclones over the open ocean distant from large landmasses. Hurricane Earl (2010) provided such an opportunity for several reasons. The NASA GRIP field campaign, coincident with two other major field campaigns in the Atlantic basin, provided extensive flight coverage of the TC, and the WWLLN captured a large number of strikes in Hurricane Earl, well over 40 000. For a lightning detection network known to have a low global detection efficiency, this was a remarkable number of strikes.

With respect to the storm motion vector, most lightning occurred left of motion in Earl, consistent with a left of motion shear vector as discussed by CM03. With respect to the shear vector, most lightning occurred downshear right in the outer rainbands and upshear left in the inner core (<100 km). The outer rainband maximum in the downshear-right quadrant agrees well with previous studies, but the inner-core, upshear-left maximum does not. Nearly all of the inner-core lightning occurred just prior to the period of RI.

Using airborne Doppler radar winds, it was found that the inner-core burst was aligned with the tilt direction of the vortex rather than with the direction of shear. During the inner-core convective burst, the vortex was tilted upshear, and the lightning was precessing counterclockwise over a 9-h period just prior to the beginning of RI. While enough observations were not available to discern if the vortex tilt was precessing with time, the initial alignment of the lightning downtilt, and the cyclonic precession of the lightning burst, suggest the tilt may have been precessing as well. Vortices are typically found to tilt in the downshear-left position because this has been shown to be the optimal configuration for tilt reduction in a sheared environment. Since prior studies have found a downshear-left tilt configuration in stronger TCs, and Earl was a developing tropical storm with an unsusual tilt, tilt configurations in sheared environments may vary depending on whether the TC is fully formed or in the process of developing.

Dropsondes revealed dry midlevel air at radii 250–450 km from the center in the upshear-left quadrant, with the most moist low levels also in this quadrant. This low-level moisture resulted in a higher average pseudoadiabatic CAPE value upshear. If this higher CAPE air was transported toward the inner core, this would help support the occurrence of deep convection and lightning upshear; however, sufficient observations were not available to confirm if this occurred. The dropsondes closer to the center of the TC, within 250 km, revealed fewer differences in low-level moisture. The RH at low levels was fairly uniform and moist in all four quadrants near the center, with a hint of dry air at midlevels left of shear. Regardless, a flight leg from the downshear-right to upshear-left quadrants of Earl revealed an environment that supported deep convection and lightning on the upshear-left side of the TC, as a strong θ_e gradient

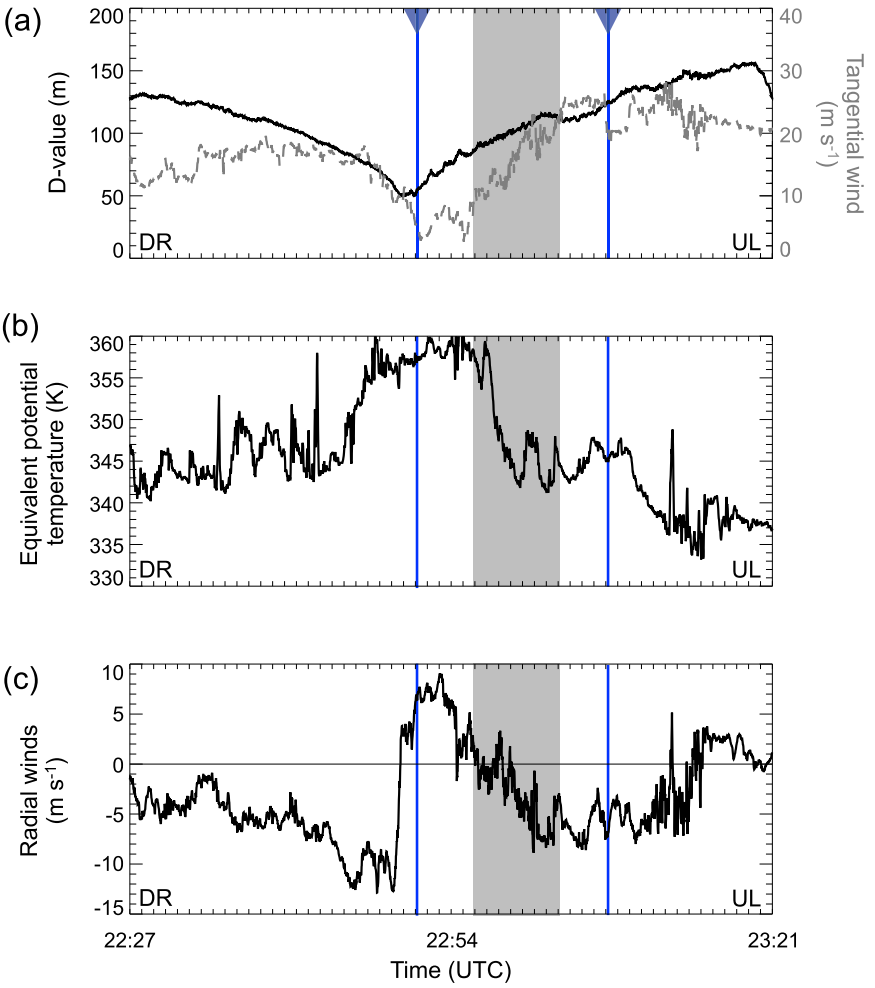

FIG. 12. Data from the NOAA43 showing flight level (a) D values (black; m) and tangential wind (gray dashed; m s^{-1}), (b) equivalent potential temperature (θ_e; K), and (c) radial winds (m s^{-1}) along the flight leg from the downshear-right to the upshear-left quadrant at approximately 675 hPa. The gray shaded area is the approximate location of the inner-core lightning burst. Blue lines indicate when dropsondes were released.

was coincident with the implied convergence of radial winds in the region where the lightning burst began.

The case of Hurricane Earl showed that an inner-core lightning burst can precede a prolonged period of RI. This burst of convection may have contributed to RI as it occurred inside the RMW, as previous studies have shown that diabatic heating sources inside the RMW lead to a spinup of the tangential wind inside the RMW, intensifying the TC. While the lightning burst occurred in an unusual quadrant, upshear left, observations revealed that this location was consistent with the vortex tilt. The role of the vertical wind shear calculated over different layers (i.e., other than the 850–200-hPa deep-layer shear) on TC convection and structure need to be explored further and is suggested for future work. Since Earl's vortex was tilted upshear left when the burst began, both the shear and diabatic heating associated with the upshear convection were likely acting to reduce the tilt, as was observed 12 h later. This alignment of the vortex in the vertical likely played a role in the subsequent period of RI. More observations of tilt configurations for intensifying TCs of varying magnitude are necessary to further address the application of vortex precession theory to observations.

Acknowledgments. The authors wish to thank the World Wide Lightning Location Network (http://wwlln.net), a collaboration among over 50 universities and institutions, for providing the lightning location data used in this paper. Flight-level, radar, and dropsonde data were obtained from the Hurricane Research Division (HRD) website. The authors thank Dan Cecil and an anonymous reviewer for comments that improved the

quality of this manuscript. The authors would also like to thank Dave Vollaro for providing shear calculations and assisting with the CAPE calculation method from the G-IV dropsondes, Philippe Papin for assisting with the area-averaged vorticity calculation method, and Robert Rogers for constructive exchanges on Earl's observations. This work was completed with NASA Hurricane Science Research Program Award NNX12AJ81G.

REFERENCES

Abarca, S. F., K. L. Corbosiero, and T. J. Galarneau Jr., 2010: An evaluation of the Worldwide Lightning Location Network (WWLLN) using the National Lightning Detection Network (NLDN) as ground truth. *J. Geophys. Res.,* **115,** D18206, doi:10.1029/2009JD013411.

——, ——, and D. Vollaro, 2011: The World Wide Lightning Location Network and convective activity in tropical cyclones. *Mon. Wea. Rev.,* **139,** 175–191, doi:10.1175/2010MWR3383.1.

Bogner, P. B., G. M. Barnes, and J. L. Franklin, 2000: Conditional instability and shear for six hurricanes over the Atlantic Ocean. *Wea. Forecasting,* **15,** 192–207, doi:10.1175/1520-0434(2000)015<0192:CIASFS>2.0.CO;2.

Braun, S. A., M. T. Montgomery, and Z. Pu, 2006: High-resolution simulation of Hurricane Bonnie (1998). Part I: The organization of eyewall vertical motion. *J. Atmos. Sci.,* **63,** 19–42, doi:10.1175/JAS3598.1.

Cangialosi, J. P., 2011: Tropical cyclone report: Hurricane Earl. National Hurricane Center Rep. AL072010, 29 pp. [Available online at http://www.nhc.noaa.gov/pdf/TCR-AL072010_Earl.pdf.]

Cecil, D. J., and E. J. Zipser, 1999: Relationship between tropical cyclone intensity and satellite-based indicators of inner core convection: 85-GHz ice-scattering signature and lightning. *Mon. Wea. Rev.,* **127,** 103–123, doi:10.1175/1520-0493(1999)127<0103:RBTCIA>2.0.CO;2.

——, ——, and S. W. Nesbitt, 2002: Reflectivity, ice scattering, and lightning characteristics of hurricane eyewalls and rainbands. Part I: Quantitative description. *Mon. Wea. Rev.,* **130,** 769–784, doi:10.1175/1520-0493(2002)130<0769:RISALC>2.0.CO;2.

Chen, S. S., J. A. Knaff, and F. D. Marks Jr., 2006: Effects of vertical wind shear and storm motion on tropical cyclone rainfall asymmetries deduced from TRMM. *Mon. Wea. Rev.,* **134,** 3190–3208, doi:10.1175/MWR3245.1.

Cline, I. M., 1926: *Tropical Cyclones*. MacMillian, 301 pp.

Corbosiero, K. L., and J. Molinari, 2002: The effects of vertical wind shear on the distribution of convection in tropical cyclones. *Mon. Wea. Rev.,* **130,** 2110–2123, doi:10.1175/1520-0493(2002)130<2110:TEOVWS>2.0.CO;2.

——, and ——, 2003: The relationship between storm motion, vertical wind shear, and convective asymmetries in tropical cyclones. *J. Atmos. Sci.,* **60,** 366–376, doi:10.1175/1520-0469(2003)060<0366:TRBSMV>2.0.CO;2.

——, ——, and M. L. Black, 2005: The structure and evolution of Hurricane Elena (1985). Part I: Symmetric intensification. *Mon. Wea. Rev.,* **133,** 2905–2921, doi:10.1175/MWR3010.1.

Cummins, K. L., and M. J. Murphy, 2009: An overview of lightning locating systems: History, techniques, and data uses, with an in depth look at the U.S. NLDN. *IEEE Trans. Electromagn. Compat.,* **51,** 499–518, doi:10.1109/TEMC.2009.2023450.

——, ——, E. A. Bardo, W. L. Hiscox, R. B. Pyle, and A. E. Pifer, 1998: A combined TOA/MDF technology upgrade of the U.S. National Lightning Detection Network. *J. Geophys. Res.,* **103,** 9035–9044, doi:10.1029/98JD00153.

Davis, C. A., S. C. Jones, and M. Riemer, 2008: Hurricane vortex dynamics during Atlantic extratropical transition. *J. Atmos. Sci.,* **65,** 714–736, doi:10.1175/2007JAS2488.1.

DeMaria, M., R. T. DeMaria, J. A. Knaff, and D. Molenar, 2012: Tropical cyclone lightning and rapid intensity change. *Mon. Wea. Rev.,* **140,** 1828–1842, doi:10.1175/MWR-D-11-00236.1.

Frank, W. M., 1977: The structure and energetics of the tropical cyclone. I. Storm structure. *Mon. Wea. Rev.,* **105,** 1119–1135, doi:10.1175/1520-0493(1977)105<1119:TSAEOT>2.0.CO;2.

Hanley, D., J. Molinari, and D. Keyser, 2001: A composite study of the interaction between tropical cyclones and upper-tropospheric troughs. *Mon. Wea. Rev.,* **129,** 2570–2584, doi:10.1175/1520-0493(2001)129<2570:ACSOTI>2.0.CO;2.

Hutchins, M. L., R. H. Holzworth, K. S. Virts, J. M. Wallace, and S. Heckman, 2013: Radiated VLF energy differences of land and oceanic lightning. *Geophys. Res. Lett.,* **40,** 2390–2394, doi:10.1002/grl.50406.

Jones, S. C., 1995: The evolution of vorticies in vertical shear. I: Initially barotropic vortices. *Quart. J. Roy. Meteor. Soc.,* **121,** 821–851, doi:10.1002/qj.49712152406.

Jorgensen, D. P., 1984: Mesoscale and convective-scale characteristics of mature hurricanes. Part II: Inner core structure of Hurricane Allen (1980). *J. Atmos. Sci.,* **41,** 1287–1311, doi:10.1175/1520-0469(1984)041<1287:MACSCO>2.0.CO;2.

——, E. J. Zipser, and M. A. LeMone, 1985: Vertical motions in intense hurricanes. *J. Atmos. Sci.,* **42,** 839–856, doi:10.1175/1520-0469(1985)042<0839:VMIIH>2.0.CO;2.

Kaplan, J., and M. DeMaria, 2003: Large-scale characteristics of rapidly intensifying tropical cyclones in the North Atlantic basin. *Wea. Forecasting,* **18,** 1093–1108, doi:10.1175/1520-0434(2003)018<1093:LCORIT>2.0.CO;2.

Landsea, C. W., and J. L. Franklin, 2013: Atlantic hurricane database uncertainty and presentation of a new database format. *Mon. Wea. Rev.,* **141,** 3576–3592, doi:10.1175/MWR-D-12-00254.1.

Lay, E. H., R. H. Holzworth, C. J. Rodger, J. N. Thomas, O. Pinto Jr., and R. L. Dowden, 2004: WWLL global lightning detection system: Regional validation study in Brazil. *Geophys. Res. Lett.,* **31,** L03102, doi:10.1029/2003GL018882.

Miller, B. I., 1958: Rainfall rates in Florida hurricanes. *Mon. Wea. Rev.,* **86,** 258–264, doi:10.1175/1520-0493(1958)086<0258:RRIFH>2.0.CO;2.

Molinari, J., and D. Vollaro, 2010: Distribution of helicity, CAPE, and shear in tropical cyclones. *J. Atmos. Sci.,* **67,** 274–284, doi:10.1175/2009JAS3090.1.

——, P. Moore, V. Idone, R. Henderson, and A. Saljoughy, 1994: Cloud-to-ground lightning in Hurricane Andrew. *J. Geophys. Res.,* **99,** 16 665–16 676, doi:10.1029/94JD00722.

——, ——, and ——, 1999: Convective structure of hurricanes as revealed by lightning locations. *Mon. Wea. Rev.,* **127,** 520–534, doi:10.1175/1520-0493(1999)127<0520:CSOHAR>2.0.CO;2.

——, D. Vollaro, and K. L. Corbosiero, 2004: Tropical cyclone formation in a sheared environment: A case study. *J. Atmos. Sci.,* **61,** 2493–2509, doi:10.1175/JAS3291.1.

——, D. M. Romps, D. Vollaro, and L. Nguyen, 2012: CAPE in tropical cyclones. *J. Atmos. Sci.,* **69,** 2452–2463, doi:10.1175/JAS-D-11-0254.1.

Montgomery, M. T., J. A. Zhang, and R. K. Smith, 2014: An analysis of the observed low-level structure of rapidly intensifying and mature Hurricane Earl (2010). *Quart. J. Roy. Meteor. Soc.,* doi:10.1002/qj.2283, in press.

Musgrave, K. D., R. K. Taft, J. L. Vigh, B. D. McNoldy, and W. H. Schubert, 2012: Time evolution of the intensity and size of tropical cyclones. *J. Adv. Model. Earth Syst.,* **4,** M08001, doi:10.1029/2011MS000104.

Nguyen, L. T., and J. Molinari, 2012: Rapid intensification of a sheared, fast-moving hurricane over the Gulf Stream. *Mon. Wea. Rev.,* **140,** 3361–3378, doi:10.1175/MWR-D-11-00293.1.

Pan, L., X. Qie, D. Liu, D. Wang, and J. Yang, 2010: The lightning activities in super typhoons over the Northwest Pacific. *Sci. China Earth Sci.,* **53,** 1241–1248, doi:10.1007/s11430-010-3034-z.

——, ——, and D. Wang, 2014: Lightning activity and its relation to the intensity of typhoons over the Northwest Pacific Ocean. *Adv. Atmos. Sci.,* **31,** 581–592, doi:10.1007/s00376-013-3115-y.

Price, C., M. Asfur, and Y. Yair, 2009: Maximum hurricane intensity preceded by increase in lightning frequency. *Nat. Geosci.,* **2,** 329–332, doi:10.1038/ngeo477.

Rappaport, E. N., and Coauthors, 2009: Advances and challenges at the National Hurricane Center. *Wea. Forecasting,* **24,** 395–419, doi:10.1175/2008WAF2222128.1.

Reasor, P. D., and M. D. Eastin, 2012: Rapidly intensifying Hurricane Guillermo (1997). Part II: Resilience in shear. *Mon. Wea. Rev.,* **140,** 425–444, doi:10.1175/MWR-D-11-00080.1.

——, M. T. Montgomery, F. D. Marks Jr., and J. F. Gamache, 2000: Low-wavenumber structure and evolution of hurricane inner core observed by airborne dual-Doppler radar. *Mon. Wea. Rev.,* **128,** 1653–1680, doi:10.1175/1520-0493(2000)128<1653:LWSAEO>2.0.CO;2.

——, ——, and L. D. Grasso, 2004: A new look at the problem of tropical cyclones in vertical shear flow: Vortex resiliency. *J. Atmos. Sci.,* **61,** 3–22, doi:10.1175/1520-0469(2004)061<0003:ANLATP>2.0.CO;2.

——, R. Rogers, and S. Lorsolo, 2013: Environmental flow impacts on tropical cyclone structure diagnosed from airborne Doppler radar composites. *Mon. Wea. Rev.,* **141,** 2949–2969, doi:10.1175/MWR-D-12-00334.1.

Rodger, C. J., J. B. Brundell, R. H. Holzworth, and E. H. Lay, 2009: Growing detection efficiency of the World Wide Lightning Location Network. Vol. 1118, *AIP Conf. Proc.: Coupling of Thunderstorms and Lightning Discharges to Near-Earth Space,* Corte, France, AIP, 15–20, doi:10.1063/1.3137706.

Rodgers, E. B., S. W. Chung, and H. F. Pierce, 1994: A satellite observational and numerical study of precipitation characteristics in western North Atlantic tropical cyclones. *J. Appl. Meteor.,* **33,** 129–139, doi:10.1175/1520-0450(1994)033<0129:ASOANS>2.0.CO;2.

Rogers, R., 2010: Convective-scale structure and evolution during a high-resolution simulation of tropical cyclone rapid intensification. *J. Atmos. Sci.,* **67,** 44–70, doi:10.1175/2009JAS3122.1.

——, S. Chen, J. Tenerelli, and H. Willoughby, 2003: A numerical study on the impact of vertical shear on the distribution of rainfall in Hurricane Bonnie (1998). *Mon. Wea. Rev.,* **131,** 1577–1599, doi:10.1175//2546.1.

——, P. Reasor, and S. Lorsolo, 2013: Airborne Doppler observations of the inner-core structural differences between intensifying and steady-state tropical cyclones. *Mon. Wea. Rev.,* **141,** 2970–2991, doi:10.1175/MWR-D-12-00357.1.

Rudlosky, S. D., and D. T. Shea, 2013: Evaluation WWLLN performance relative to TRMM/LIS. *Geophys. Res. Lett.,* **40,** 2344–2348, doi:10.1002/grl.50428.

Samsury, C. E., and R. E. Orville, 1994: Cloud-to-ground lightning in tropical cyclones: A study of Hurricanes Hugo (1989) and Jerry (1989). *Mon. Wea. Rev.,* **122,** 1887–1896, doi:10.1175/1520-0493(1994)122<1887:CTGLIT>2.0.CO;2.

Shapiro, L. J., and H. E. Willoughby, 1982: The response of balanced hurricanes to local sources of heat and momentum. *J. Atmos. Sci.,* **39,** 378–394, doi:10.1175/1520-0469(1982)039<0378:TROBHT>2.0.CO;2.

Thomas, J. N., N. N. Solorzano, S. A. Cummer, and R. H. Holzworth, 2010: Polarity and energetics of inner core lightning in three intense North Atlantic hurricanes. *J. Geophys. Res.,* **115,** A00E15, doi:10.1029/2009JA014777.

Vigh, J. L., and W. H. Schubert, 2009: Rapid development of the tropical cyclone warm core. *J. Atmos. Sci.,* **66,** 3335–3350, doi:10.1175/2009JAS3092.1.

Virts, K. S., J. M. Wallace, M. L. Hutchins, and R. Holzworth, 2013: Highlights of a new ground-based, hourly global lightning climatology. *Bull. Amer. Meteor. Soc.,* **94,** 1381–1391, doi:10.1175/BAMS-D-12-00082.1.

Wang, Y., and G. J. Holland, 1996: Tropical cyclone motion and evolution in vertical shear. *J. Atmos. Sci.,* **53,** 3313–3332, doi:10.1175/1520-0469(1996)053<3313:TCMAEI>2.0.CO;2.

Wu, L., S. A. Braun, J. Halverson, and G. Heymsfield, 2006: A numerical study of Hurricane Erin (2001). Part I: Model verification and storm evolution. *J. Atmos. Sci.,* **63,** 65–86, doi:10.1175/JAS3597.1.